ACS APPLIED MATERIALS & INTERFACES

www.acsami.org

Research Article

Peculiarities of Redox Catalysis With Peroxidase-Like Nanozymes

Published as part of ACS Applied Materials & Interfaces special issue "Nanozymes: Design, Mechanisms, and Applications".

Maria A. Komkova,* Aleksandra A. Shneiderman, Elena S. Povaga, Yuting Wang, Xiwen Chen, Alexander L. Kustov, Congzhong Yang, Hui Wei, and Arkady A. Karyakin

Cite This: *ACS Appl. Mater. Interfaces* 2025, 17, 40964−40973

Read Online

ACCESS | Metrics & More | Article Recommendations | Supporting Information

ABSTRACT: Catalytic pathways of peroxidase-like nanozymes based on different nanomaterials are critically compared. For all nanomaterials, the catalytic rate constant (k_{cat}) for reducing substrate is increased as the redox potential of the nanozyme itself is increased: 100 mV rise in the catalyst's redox potential provides 1000 times higher k_{cat}. Logarithm of the catalytic constant as a function of both nanozyme and substrate redox potentials for Prussian Blue belongs to the same trend as for the enzyme peroxidase, whereas other materials (Fe_3O_4, CeO_2, and $LiFePO_4$) display significantly lower activity. Size-dependence of catalytic constant returns the slope from 2.6 to 2.8 in double logarithmic plots, indicating penetration of hydrogen peroxide to the bulk of nanozymes. The electrochemical rate constant, on the contrary, is much higher for smaller nanozymes, pointing to more dense packing of the electrocatalytic layer. Catalytically synthesized Prussian Blue nanozymes are successfully applied for ROS scavenging in living cells.

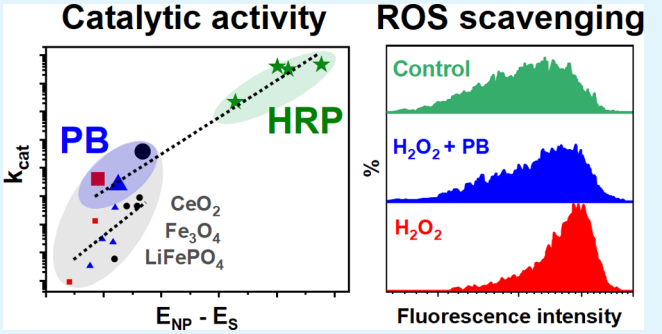

KEYWORDS: *nanozyme, artificial peroxidase, redox catalysis, electrocatalysis, H_2O_2 reduction, ROS scavenging*

1. INTRODUCTION

The neologism "nanozyme" was introduced 20 years ago for the triazacyclonane/Zn^{2+} complexes on gold nanoparticles with ribonuclease-like activity,[1] following the same naming pattern as "ribozyme" or "abzyme". The term has already become firmly established for nanomaterials with enzyme-like activity, whereas "nanozymology" evolved into a separate scientific field bridging nanotechnology and enzymology.[2]

Inspired by natural biocatalysts, numerous nanomaterials with oxidoreductase-like activities have been developed, including the mimetics of peroxidase, catalase, superoxide dismutase, hydrolase, etc. Triggered by the first evidence of the peroxidase-like activity for the ferromagnetic nanoparticles,[3] an avalanche of 'artificial peroxidase' related papers has been issued. This is not surprising, since such nanoparticles have appeared to be efficient as natural enzyme substitutes in various spheres, from biosensing to tumor theranostics.[4] Except for metal oxides, metal nanoparticles, metal−organic frameworks, and various carbon nanomaterials have been reported to mimic peroxidase.[2] Although it is not feasible to list all of them, the nanozymes based on nitrogen-coordinated iron atoms (including the so-called single-atom nanozymes) probably possess the highest activity.[5]

The incredible rise of investigations devoted to nanoparticles with enzyme-like activity gave way to a number of critical reviews casting doubt on the concept and definition of nanozymes.[6,7] In particular, the opponents have underscored the ability of inorganic nanomaterials to decompose H_2O_2 unrelated to enzymatic catalysis, which had been known for decades.[8] Indeed, the majority of studies are more descriptive of nanozyme characteristics, while the mechanism of their action as catalysts, which may differ from those of their enzyme counterparts, is omitted.

Several attempts have been made to standardize the assays for determining the catalytic activity of various nanozymes for their correct quantitative comparison.[9,10] The authors paid much attention to activity calculations with respect to nanozyme surface area, shape, and size and suggested recalculation using a number of active sites determined by chemosorption. Nevertheless, the recommended pH value below 4.0 as well as H_2O_2 concentration of 1.0 M simply replicate the conditions found optimal for magnetite nano-

Received: April 14, 2025
Revised: June 26, 2025
Accepted: June 27, 2025
Published: July 8, 2025

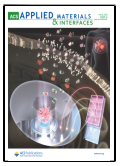

particles earlier[3] and seem inappropriate for peroxidase mimicking. Indeed, for natural peroxidases, an apparent Michaelis constant for H_2O_2 does not exceed 10 mM, while pH 5.0−6.0 is considered optimal for the enzyme.[11] Moreover, according to the Pourbaix diagram for the iron−water system,[12] the magnetite phase is thermodynamically unstable at pH below 5.0. Hence, peroxidase activity observed for Fe_3O_4 nanoparticles stored in acidic media (down to pH < 1.0) is probably due to the presence of other phases, which are stable under the given conditions.

With the current investigation, we plan to unify the physicochemical principles of peroxide reduction catalysis with different nanomaterials. Probably the most used peroxidase-mimicking nanozymes based on iron oxide (Fe_3O_4) and cerium oxide (CeO_2) nanoparticles have been chosen. Although nanozymes originate from magnetite nanoparticles,[3] the nature of their observed catalytic activity is still being debated.[13] Cerium oxides are generally applied for therapeutic applications.[14,15] However, these particles are credited with multienzyme activity.[16,17] Accordingly, while most studies are aimed at obtaining high total ROS scavenging activity, the mechanism of hydrogen peroxide reduction has received little attention. Except for oxide-based nanozymes, a set of other transition metal-based nanomaterials and complexes was considered. Particular attention was paid to catalytically synthesized Prussian Blue,[11] demonstrating outstanding catalytic properties and even denoted as "artificial peroxidase".

Evidently, considering oxidoreductase mimicking, one would expect a strong influence of both the substrate and nanozyme redox potentials on the turnover number. Accordingly, we suggest investigating peculiarities of catalysis with electroactive nanomaterials in terms of their intrinsic redox activity, as well as electron-donor properties of the substrates. Moreover, it is expected that highly electroactive nanomaterials with superior catalytic activity would provide efficient electrocatalysis similar to direct bioelectrocatalysis with peroxidases.[18] Unlike the enzymes, which form a monolayer at the electrode interface, which can be potentially involved in direct electron transfer, the use of electroactive nanomaterials would allow involving a larger number of active sites in the reaction. A critical comparison of redox catalysis peculiarities for different nanoparticles performed in the article would allow us to distinguish the most promising catalysts, which deserve to be called "artificial peroxidase" and guide the design of new peroxidase-like nanozymes for a wide range of applications, from electrochemical sensing to anti-inflammatory therapy.

2. MATERIALS AND METHODS

Materials and Equipment. Hydrogen peroxide (30% solution), potassium ferricyanide, iron(III) chloride hexahydrate, catechol, *o*-phenylenediamine, and 3,3′,5,5′-tetramethylbenzidine (TMB) at the highest purity were purchased from Sigma Aldrich (USA) and used as received. $Fe(C_5H_7O_2)_3$−Fe(III) acetylacetonate (99+%) from Acros Organics and C_7H_8O−benzyl alcohol (99%) from Alfa Aesar were used as received. Cerium nitrate hexahydrate (99.95%), ethylene glycol (analytically pure, 98%), concentrated ammonia solution (analytically pure, 25−28%), and 2′,7′-dichlorofluorescin diacetate (DCFH-DA) were obtained from Shanghai Aladdin Biochemical Technology Co., Ltd. Dulbecco's modified Eagle medium (DMEM), fetal bovine serum (FBS), penicillin, and streptomycin solution were purchased from Gibco. RAW 264.7 cells were purchased from the Cell Bank of the Chinese Academy of Sciences (Shanghai, China). The cells were cultured in high-glucose DMEM (Shenghang Bio, China) supplemented with 10% (v/v) FBS and 1% penicillin/streptomycin (Cytiva, USA) at 37 °C in a 5% CO_2 incubator. CCK-8 solution was purchased from Dojindo. Horseradish peroxidase (EC 1.11.1.7), type VI (activity ≥ 250 pyrogallol units/mg), from Sigma Aldrich (USA) was used. Iron(III) in 0.1 M HNO_3 standard (no. 7765−2000, Ecoanalytica, Russia) was used for inductively coupled plasma mass spectrometry (ICP-MS) measurements. Alumina powder with a particle size of 50 nm by Sigma-Aldrich (USA) was used for the glassy carbon electrode polishing.

Synthesis of Prussian Blue nanostructures was carried out in a PSB-Gals (Russia) ultrasonic bath. Centrifuge Eppendorf MiniSpin (Eppendorf, Germany) was used for nanoparticle separation. Estimation of size and analysis of nanozymes microstructure was carried out using a transmission electron microscope, Libra 200 (Carl Zeiss, Germany). X-ray powder diffraction experiments were performed using a HUBER G670 Guinier camera (CoKα1 radiation, λ = 1.78965 Å) for Prussian Blue-based nanozymes and using a D/MAX-2500V/PC diffractometer (Rigaku Corporation, Japan, CuKα1 radiation, λ = 1.5406 Å) for the other nanoparticles. Elemental analysis and estimation of the materials' concentrations in the colloidal solutions were carried out using ICP-MS Elan DRC II (PerkinElmer, USA). In the case of powders, colloids were prepared by weighing. The UV/vis absorption measurements in transmission mode, including steady-state kinetics measurements, were carried out using a Lambda 950 Spectrophotometer (PerkinElmer, USA). Electrochemical measurements were performed using a PalmSens 4 potentiostat (PalmSens BV, The Netherlands). For the square-wave voltammetry measurements, glassy carbon disk electrodes (d = 1.0 mm) by Beijing Jingke Scientific Instrument Co., Ltd. (China) were used. For hydrodynamic and kinetic measurements, planar screen-printed structures with a graphite working electrode (d = 1.8 mm) by Ltd. Rusens (Russia) were used. A self-made flow-through wall-jet cell with a 0.5 mm nozzle positioned at 1.0 mm distance from the surface of the disk electrode connected to the syringe pump Braun Perfusor (Germany) was applied for hydrodynamic measurements. A flow cytometer CyoFLEX (Beckman Coulter, USA) was used for evaluation of nanozymes' activity in ROS scavenging.

Microwave-Assisted Synthesis of Fe_3O_4 Nanoparticles. One g portion of Fe(III) acetylacetonate was dissolved in 45 mL of benzyl alcohol in the beaker. The solution was placed in the domestic microwave oven Midea AM820CMF. The microwave treatment was carried out for 1 h under the following conditions: 900 W, 190 °C, and atmospheric pressure. The obtained precipitate was separated by the neodymium magnet, washed with ethanol, and dried under vacuum for 4 h at 40 °C.

Synthesis of CeO_2 Nanoparticles. CeO_2 nanoparticles were synthesized via a hydrothermal method. Initially, 126 mg of $Ce(NO_3)_3{\cdot}6H_2O$ was dissolved in 10 mL of ethylene glycol to prepare a homogeneous solution. This solution was then gradually added to 10 mL of deionized water under vigorous stirring for 5 min. The resulting mixture was maintained in a 60 °C water bath with continuous stirring for an additional 10 min. Subsequently, 1.6 mL of concentrated ammonia solution (28−30%) was swiftly introduced into the mixture using a syringe. The reaction was allowed to proceed under continuous stirring at 60 °C for 3 h. The synthesized CeO_2 nanoparticles were collected by centrifugation and thoroughly washed with water multiple times until the pH of the supernatant reached neutrality. Finally, the CeO_2 product was redispersed in the water.

Catalytic Synthesis of Prussian Blue Nanoparticles. Prussian Blue nanoparticles with sizes ranging from 32 to 360 nm were synthesized catalytically as described in ref 11. A soluble complex $Fe^{III}[Fe^{III}(CN)_6]$ formed by 1:1 mixing of Fe^{3+} and $[Fe(CN)_6]^{3-}$ (5−75 mM in 0.1 M KCl/0.1 M HCl solution, pH = 1.1) was reduced by H_2O_2 (20−50 mM) upon ultrasonication during 0.5−20 min. In the course of Prussian Blue precipitation, the red-brown color of the iron (III) ferricyanide complex changes to dark blue (Figure S1). The synthesized particles were separated by centrifugation at 13000 r.p.m. for 0.5 min. Then the obtained precipitates were redispersed into 0.1 M KCl/0.1 M HCl solution (the procedure of centrifugation−redispersion was repeated 5−7 times). The catalytically synthesized

https://doi.org/10.1021/acsami.5c07510
ACS Appl. Mater. Interfaces 2025, 17, 40964−40973

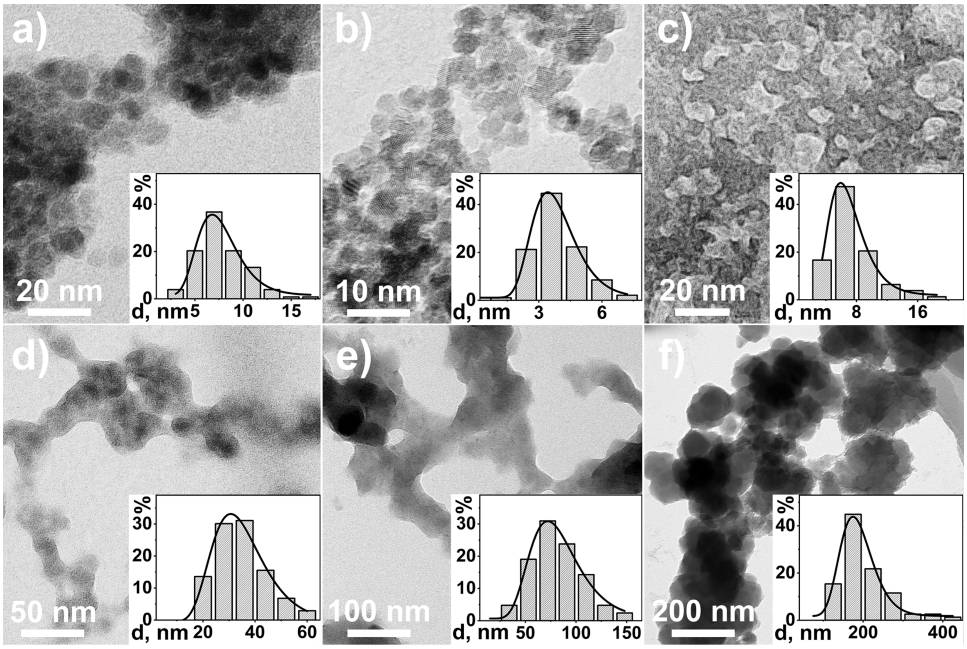

Figure 1. TEM images of nanozymes based on (a) Fe_3O_4, (b) CeO_2, (c) $LiFePO_4$, and Prussian Blue-based nanozymes with sizes of (d) 34, (e) 80, and (f) 185 nm. The size distribution of nanozymes, obtained from a set of micrographs, is given in the insets.

nanoparticles were stored at pH = 1.1 and ultrasonicated prior to use. Concentrations of Prussian Blue nanozymes with different sizes in colloidal solutions were calculated considering elemental analysis and electron microscopy data. The diameters of at least 100 nanoparticles were used to build their size distributions.

BET Analysis. Colloids of Prussian Blue-based nanozyme sizing from 32 to 190 nm were thoroughly washed with 0.01 M HCl and dried at 100 °C prior to measurement. A Quantachrome Nova 4200e instrument was utilized for surface analysis using N_2 at 77 K as a working gas. To extract specific surface area and porosity of the samples, the isotherms were treated using a conventional procedure based on Brunauer–Emmett–Teller (BET) theory.

X-ray Photoelectron Spectroscopy (XPS). XPS measurements were performed by using a PREVAC EA15 spectrometer (PREVAC, Rogów, Poland). In the current work, Al Kα radiation ($h\nu$ = 1486.6 eV, 150 W) was used as a primary radiation source. The pressure in the analytical chamber did not exceed 5×10^{-9} mbar during spectra acquisition. The binding energy scale was precalibrated using the positions of Ag $3d_{5/2}$ (368.3 eV) and Au $4f_{7/2}$ (84.0 eV) from silver and gold foils, respectively. Nanoparticle samples were deposited from a buffer solution, dried under vacuum, and then introduced into the chamber. To take into account the effect of surface charging, the C 1s line (E_b = 284.8 eV) from the carbon contamination was used as an internal standard.

Redox and Electrocatalytic Activity Investigation. Electrochemical investigations were carried out in a three-electrode setup with a glassy carbon or screen-printed graphite working electrode, Ag|AgCl|1 M KCl reference electrode, and glassy carbon rod counter electrode. Prior to nanozyme adsorption, the glassy carbon working electrode was mechanically polished in a water suspension of alumina to a mirror finish, and a stable voltammogram with minimum capacitance in the buffer solution was obtained. Different electroactive nanoparticles were immobilized by a simple drop-casting of the corresponding colloids with subsequent heating at 60 °C for 15 min. Their electroactivity was investigated in the square-wave voltammetry regime. Voltammograms were recorded with an amplitude of 0.05 V, potential step of 1.0 mV, and frequency of 1.0 Hz. For investigation of pH dependence of Fe_3O_4 electroactivity in the square-wave voltammetry mode, pH values were adjusted using 0.05 M borate, phosphate-citrate, acetate buffer solutions, or hydrochloric acid solution.

Electrocatalytic performances were investigated using nanoparticle-modified glassy carbon electrodes integrated into the flow-through wall-jet cell. Hydrodynamic voltammograms of H_2O_2 electrocatalytic reduction were registered at a flow rate of 20 mL·h^{-1}. To distinguish the current terms controlled by diffusion and kinetics and determine the electrochemical rate constant k_{el}, the volume flow rates were varied in the range from 36 to 120 mL·h^{-1}.

Investigation of Peroxidase-Like Activity. Steady-state kinetics measurements were carried out at room temperature in buffer solutions, containing 0.05–10 mM of H_2O_2, 0.5 μM–50 mM of reducing substrate (depending on the nature of the substrate), and 0.2–100 μM of electroactive material (overall concentration in the colloidal solution). Phosphate-citrate buffer solution (pH = 5.0) was used, maintaining the pH value in the range, which is optimal for natural peroxidases (pH = 5.0–6.0). The concentration of the oxidized substrate was monitored spectrophotometrically immediately after injection of nanozymes into the H_2O_2-reducing substrate mixture. The molar extinction coefficients: $\varepsilon(K_3[Fe(CN)_6]$, 420 nm) = 1.04×10^3 M^{-1}·cm^{-1}, ε(2,3-diaminophenazine, 450 nm) = 1.1×10^4 M^{-1}·cm^{-1}, (quinone, 390 nm) = 1.37×10^3 M^{-1}·cm^{-1}, ε(*o*-dianisidine oxidized, 440 nm) = 1.13×10^4 M^{-1}·cm^{-1}, $\varepsilon(TMB^{2+}$, 450 nm) = 5.9×10^4 M^{-1}·cm^{-1}, were used to evaluate the initial reaction rates. The latter was calculated using the slope of absorption against time dependencies. Oxidase activity was evaluated by considering the substrate oxidation with dissolved oxygen (~0.2 mM) in the absence of H_2O_2.

Cytotoxicity Evaluation. To evaluate cell viability, RAW 264.7 cells were seeded in 96-well plates at a density of 5000–10000 cells per well. After overnight incubation, the culture medium was replaced with fresh medium containing different concentrations (0–344 μg·mL^{-1}) of Prussian Blue, and nanozymes with different sizes were used. Following an additional 24–48 h incubation, the cells were washed three times with PBS. Cell viability was assessed using the CCK-8 assay (n = 3) according to the manufacturer's instructions, and absorbance was measured using a microplate reader.

Cell viability was calculated using the following formula:

$$\text{cell viability} = (O_t - O_b)/(O_c - O_b) \times 100\%$$

where O_t represents the absorbance of the nanozyme-treated group, O_b represents the absorbance of the blank group (without cells), and

https://doi.org/10.1021/acsami.5c07510
ACS Appl. Mater. Interfaces 2025, 17, 40964–40973

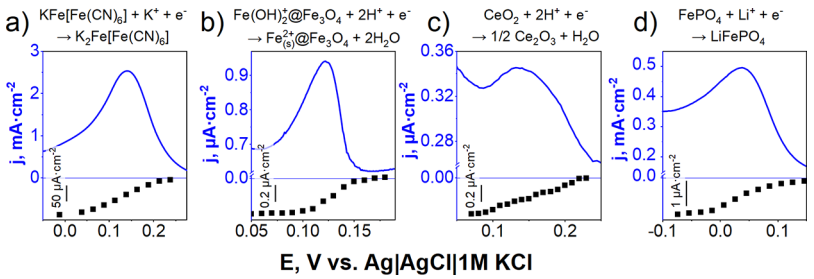

Figure 2. Square wave voltammograms of electroactive nanomaterials adsorbed on the surface of glassy carbon electrodes: 79 nmol·cm^{-2} of Prussian Blue (a) and 0.79 μmol·cm^{-2} of Fe_3O_4 (b), CeO_2 (c), $LiFePO_4$ (d) and the hydrodynamic voltammograms of 0.2 mM H_2O_2 reduction at their surface; 0.05 M citrate-phosphate buffer, pH = 5.0.

O_c represents the absorbance of the control group (cells without material treatment).

Evaluation of ROS Scavenging Activity. To evaluate the ROS scavenging activity of catalytically synthesized Prussian Blue nanoparticles, RAW 264.7 cells were seeded in 12-well plates at a density of 1×10^4 cells per well and incubated in DMEM for 24 h. The cells were then treated with fresh medium containing 5 or 10 μg·mL^{-1} of Prussian Blue nanoparticles and incubated for 3 h. Following three washes with PBS, all groups, except for the negative control, were exposed to H_2O_2 (0.1 mM) for 30 min to induce intracellular ROS generation. After stimulation, the cells were washed three times with fresh medium and subsequently incubated with DCFH-DA (0.01 mM) in serum-free, phenol red-free medium for 20 min. Once internalized, DCFH-DA is hydrolyzed by intracellular esterases to form dichlorodihydrofluorescein (DCFH), which is then oxidized by ROS into fluorescent dichlorofluorescein (DCF), exhibiting excitation and emission at 488 and 520 nm, respectively. The cells were then washed three times with PBS to remove excess probe, collected by centrifugation, and analyzed via flow cytometry to quantify intracellular ROS levels.

ROS scavenging was confirmed with the fluorescence images recorded by a Nikon Ti confocal microscope Nikon Ti (Japan). To visualize ROS localization in cells (shown in green), DCFH-DA staining was applied. The cells themselves were stained with Hoechst (imaged in blue). Prior to measurement, DCFH-DA and Hoechst (both 0.01 mM) in DMEM (with no FBS) were added to each well plate for 30 min followed by washing with PBS 3 times.

3. RESULTS AND DISCUSSION

Synthesis and Investigation of Nanoscale Electroactive Particles. In the current research, we consider a set of electroactive nanomaterials based on transition metal ions as peroxidase mimetics. Catalysis of H_2O_2 reduction with such materials is expected to occur via transition metal redox reactions similar to those in the peroxidase prosthetic group heme. Accordingly, we investigated probably the most widely used peroxidase mimetics based on iron (II, III) oxide (Fe_3O_4) and cerium oxide (CeO_2). Taking into account that heme contains an iron atom, in addition to Fe_3O_4 nanoparticles, a number of nanostructures based on iron coordination materials, including lithium iron phosphate ($LiFePO_4$) and ferric hexacyanoferrate ($KFe[Fe(CN)_6]$, Prussian Blue), were tested.

Nanoparticles of transition metal oxides (Fe_3O_4 and CeO_2) were synthesized using a solvothermal method, which allows obtaining nanostructures with a narrow size distribution and reproducible properties. According to transmission electron microscopy data, the synthesized magnetite and cerium oxide nanoparticles represent slightly agglomerated structures with average sizes of about 6 and 4 nm, respectively (Figure 1a, b). PDI values do not exceed 0.09 (Figure S2), and thus, the samples can be referred to as narrow-dispersed ones. The X-ray powder diffraction patterns of the dried samples (Figure S3a,b) indicate that the nanostructures of iron oxide with magnetite spinel structure (JCPDF no. 88−0315, cubic, $Fd\bar{3}m$) and cerium oxide with fluorite crystal lattice (JCPDF no. 34−0394, cubic, $Fm\bar{3}m$) were formed. The mean size of crystalline domains, estimated using the Scherrer equation and considering the half-width of the (200) reflection in the case of Fe_3O_4 and the (111) reflection in the case of CeO_2, coincides with the average size of individual grains determined by TEM. The latter, thus, can be considered monocrystalline. Nevertheless, in water electrolytes, such particles tend to agglomerate, resulting in a higher hydrodynamic size of colloidal structures (Figure S4a,b).

The particles of commercially available lithium iron (II) phosphate powder with an olivine crystal structure, generally used for lithium-ion battery manufacturing, were also investigated. According to TEM micrographs, the powder consists of strongly agglomerated 8 nm particles (Figure 1c).

Prussian Blue-based nanoparticles were synthesized catalytically, reducing soluble ferric ferricyanide complex $Fe^{III}[Fe^{III}(CN)_6]$ (a structural analog of Berlin Green, the catalyst of H_2O_2 oxidation), as we proposed earlier.[11] Such an approach allows tuning the size of the synthesized nanozymes by simply varying the concentrations of precursors, so that concentrated growing solutions and faster precipitation result in smaller particles (the size is probably adjusted by the ratio of nucleation and crystal growth rates). The Prussian Blue-based nanozymes with the diameter ranging roughly from 30 to 350 nm were obtained (Figure 1d−f). Due to rather high surface energy and low zeta potential (ζ = (20−25) mV)) of Prussian Blue nanostructures, it is rather complicated to obtain smaller particles without any template or stabilizing shell. The X-ray powder diffraction of the synthesized nanoparticles with various sizes confirms that their crystalline structure is typical for Prussian Blue (record 73−0687 JCPDS, Figure S3c).

The catalytically synthesized moderately dispersed (Figure S2) nanoparticles are not monocrystalline and consist of smaller grains. The size of the latter, as well as coherent scattering region values, depend on the nanozyme diameter. According to electron microscopy data (Figure 1d−f), the nanozymes with a size of 34 nm consist of 8−9 nm grains (according to Scherrer's equation, half-width of (200) reflection considered), while larger nanozymes of about 200 nm represent the agglomerates of 50−70 nm structures. Coherent scattering region values, calculated according to X-ray diffraction data (Figure S3), are even smaller but change sequentially from 9 to 19 nm. Such polycrystalline nanozymes are stable in solution, resulting in a reproducible hydrodynamic size distribution (according to DLS data, Figure S4c,e), so that

https://doi.org/10.1021/acsami.5c07510
ACS Appl. Mater. Interfaces 2025, 17, 40964−40973

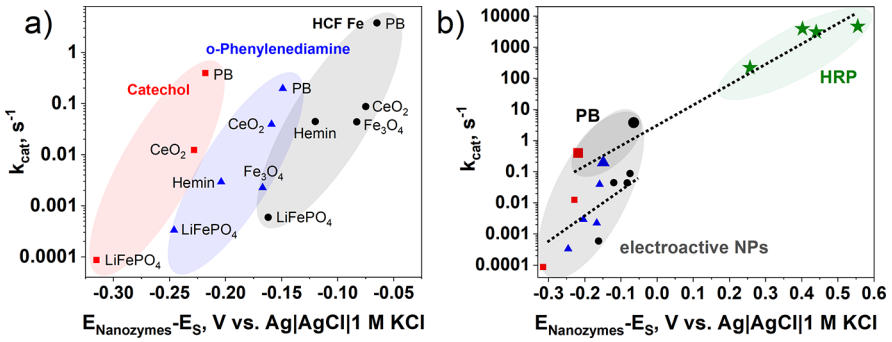

Figure 3. (a) Catalytic rate constants k_{cat} for reducing substrates: $K_4[Fe(CN)_6]$ (black), *o*-phenylenediamine (blue), catechol (red), normalized to a number of potentially electroactive sites depending on the intrinsic electroactivity of nanozymes and the reducing ability of the substrate. (b) Trends of the corresponding k_{cat} values depending on the catalyst (HRP redox potential from ref 22 was used) and the substrate redox potentials for electroactive nanoparticles and natural enzyme peroxidase (stars); 2.0 mM H_2O_2, 0.05 M citrate-phosphate buffer, pH 5.0.

the mean size coincides with the average diameter estimated using electron microscopy data within the error tolerances. Therefore, by the size of the Prussian Blue-based nanozyme, we mean the diameter of the polycrystalline colloidal nanoparticle.

According to BET adsorption data (Table S1), the porosity of Prussian Blue-based nanozymes (average 0.3 $cm^3 \cdot g^{-1}$) is practically independent of their diameter. At the same time, the samples possess a high specific surface area, slightly growing with their size (roughly from 305 to 365 $m^2 \cdot g^{-1}$). We expect that both high porosity and microstructure of nanozymes, representing ensembles of smaller grains, would promote efficient mass transport in their bulk.

The considered nanomaterials are expected to display intrinsic electroactivity in aqueous electrolytes. Indeed, for the nanoparticles immobilized on the surface of graphite electrodes, an explicit peak of their redox transitions is observed in the square-wave voltammograms (Figure 2). The highest redox activity was achieved for Prussian Blue-based nanozymes. As we have shown earlier, up to 60% of the material can be involved in the Prussian Blue/Prussian White redox transition depending on the nanoparticles' size (packing density in the film).[19] Such a substantial fraction of electroactive material can be achieved only in the case when the redox process occurs in the bulk of the particles. For $LiFePO_4$, generally applied as a cathode material in lithium-ion batteries (when Li^+ intercalation is accompanied by iron redox reaction), a significant fraction of the immobilized material stays electroactive even in aqueous electrolytes. On its turn, oxide particles display rather low redox activity: the electroactive fraction of immobilized materials does not exceed 1%, which is probably related to their poor electronic conductivity. For such nanoparticles, the reaction would occur exclusively on their surface. However, due to their small size (several unit cells in diameter) and high surface-to-volume ratio, such low conductivity is not expected to limit the peroxidase-like catalysis significantly.

Unraveling the mechanism of nanomaterials' peroxidase-like action, we suggest, first of all, to consider the thermodynamics of H_2O_2 reduction on their surface. Figure 2 displays hydrodynamic voltammograms of H_2O_2 reduction for Prussian Blue, $LiFePO_4$, Fe_3O_4, and CeO_2 nanoparticle modified electrodes. As known, Prussian Blue acts as a redox catalyst, whereas its semioxidized ground state is silent in electrocatalysis, and the reduction of H_2O_2 is catalyzed only with its reduced form (Prussian White).[20] Accordingly, the half-wave potential of H_2O_2 reduction at the electrode modified with Prussian Blue-based nanozymes almost coincides with the Prussian Blue/Prussian White redox potential (Figure 2, Figure S5). Similar behavior is observed in the case of electrocatalysis with adsorbed nanoparticles of $LiFePO_4$ and oxides, for which $E_{1/2}$ perfectly matches the peak potential in the square-wave voltammograms (Figure S5). We also note that the potential of H_2O_2 reduction to H_2O at pH = 5.0 equals 1.25 V vs Ag/AgCl/1 M KCl.[21] Hence, in the potential window of the considered materials' redox activity (below 0.2 V vs Ag/AgCl/1 M KCl, Figure 2) the current of H_2O_2 reduction has to reach its saturation. Accordingly, the half-wave potential for the hydrodynamic voltammogram of H_2O_2 reduction is determined by the properties of the electrocatalysts.

To attribute the observed electroactivity of magnetite and associated electrocatalysis to a certain redox reaction, we turned to Pourbaix diagrams for the iron−water system.[12] Taking into account the slope of peak potential−pH dependence (about 122 mV per pH unit in the range from pH 9.0 down to pH = 5.0, tending to 0 mV per pH unit in strong acidic conditions) as well as absolute formal potential values (Figure S6), we assume that the observed redox catalysis is not driven by the magnetite redox transition itself. Probably, the electrocatalytic process occurs through the equilibrium of $Fe(OH)_2^+$ and $Fe^{2+}(s)$ species adsorbed at the Fe_3O_4 interface. The same species are expected to participate in the catalytic reaction of H_2O_2 reduction in the presence of the electron-donor substrates.

The as-synthesized nanomaterials, except for lithium iron phosphate, exist in an oxidized/semioxidized state. Nonetheless, according to open circuit potential measurements both in freshly prepared and aged colloids, $LiFePO_4$ appears to be partially oxidized upon lithium deintercalation. Indeed, according to XPS analysis of nanozyme surface in freshly prepared colloids in phosphate-citrate buffer, the ratios of oxidized and reduced transition metal ions tend to the values expected to be achieved at their formal redox potentials, which is predictable for electroactive materials. Nevertheless, these ratios still exceed the theoretical values, which indicates that the surface is oxidized rather than reduced (Figure S7, Table S2). Since H_2O_2 can be reduced only with the reduced form of electroactive nanomaterials, the nanozymes under consideration have to react with the electron-donor substrate initially.

The steady-state kinetics approach was used to evaluate the catalytic activity of the nanoparticles in H_2O_2 reduction catalysis. The latter was investigated using electron-donor

https://doi.org/10.1021/acsami.5c07510
ACS Appl. Mater. Interfaces 2025, 17, 40964−40973

peroxidase substrates with different reducing ability, including potassium ferrocyanide ($K_4[Fe(CN)_6]$, $E^{0\prime}$ = 0.205 V), *o*-phenylenediamine ($E^{0\prime}$ = 0.29 V), catechol ($E^{0\prime}$ = 0.355 V), and o-dianisidine ($E^{0\prime}$ = 0.43 V). As shown, the initial reaction rate obeys the hyperbolic dependence on the substrate concentration, while it has been found to be a linear function of the nanozymes' concentration intersecting the origin (Figure S8). It confirms the validity of the Michaelis−Menten equation ($v = \frac{k_{cat}[E]_0[S]_0}{K_M^{app} + [S]_0}$) for the formal analysis of the nanozyme-catalyzed reactions and evaluation of catalytic rate constants k_{cat}.

Figure 3a displays the catalytic constants (k_{cat}) per single potentially electroactive site as a function of the difference between the nanomaterial and substrate redox potentials. Except for electroactive nanoparticles, we have provided data on the catalytic activity of hemin ($E^{0\prime}$ (pH = 5.0) = 0.085 V[23]) in the presence of the "fastest" substrates. The catalytic constants for the reducing substrates were determined in the presence of 2.0 mM H_2O_2, given that at this concentration, the enzyme horseradish peroxidase's apparent catalytic constant becomes substrate-saturated. Meanwhile, for the considered electroactive nanomaterials, the catalytic constant for the reducing substrate is linearly dependent on H_2O_2 concentration (Figure S9). The data sets for catalytic rate constants determined for different nanomaterials form separate trends, depending on the type of reducing agent (Figure 3). In addition to iron-containing nanozymes, the catalytic constants for cerium oxide also fit these trends. Expectedly, higher redox potential of the substrate results in lower k_{cat} values. An increase in $E^{0\prime}$ of the substrate redox potential by 150 mV leads to a decrease in the catalytic constant value by almost an order of magnitude (Figure 3a). Even a stronger impact of nanozyme electroactivity was demonstrated. As shown, a decrease in the catalyst redox potential by only 100 mV increases the catalytic rate constant by ∼3 orders of magnitude. Although it is rather complicated to evaluate the redox-potential for the nanomaterials with low electroactivity, to demonstrate the versatility of the observed trends, we also provided data on k_{cat} as a function of the difference between the nanomaterial and the substrate redox potential for a wider range of transition metal-based nanomaterials and complexes (Figure S10). Among the considered nanomaterials, the highest catalytic activity was achieved for the Prussian Blue catalyst independently of the reducing substrate (Figure 3a).

Considering the peroxidase-like activity of nanozymes, a question that naturally arises is how the achieved turnover numbers relate to the activity of the enzyme. Similarly to electroactive nanoparticles, the activity of the natural enzyme tends to increase, reducing the substrate redox potential (Figure 3b). Expectedly, catalytic activities comparable to those of the enzyme are unattainable for a single active center of an electroactive nanoparticle. Nevertheless, it is noteworthy that catalytic constants as a function of $(E^{0\prime}{}_{\text{nanozyme}} - E^{0\prime}{}_{S})$ for HRP and Prussian Blue seem to belong to the same trend (Figure 3b). At the same time, the other considered catalysts demonstrate dramatically lower activities, which do not fit into it. One can assume that, except for the redox potential of the nanozyme material, the coordination of the electroactive atom is also important. Indeed, the structure of the nitrogen-coordinated high-spin iron atom in Prussian Blue is similar to that of the iron atom in peroxidase heme. In addition, the maximum activity among peroxidase mimetics has been observed for the Fe−N−C catalysts.[5] Nevertheless, heme itself, separately from the protein globule, does not possess high peroxidase activity. This is also implicitly confirmed by the value of catalytic constant for hemin, which is 100 times lower than for Prussian Blue-based nanozymes and 4 orders of magnitude lower than for peroxidase (Figure 3a).

While high intrinsic selectivity is among the main advantages of enzymes, unfortunately, for a number of nanozymes, a multienzyme activity had been observed. For instance, the ability of nanozymes to catalyze oxygen reduction with the substrate in the absence of H_2O_2 (oxidase-like activity) should be taken into account. As shown, even using the substrate with the lowest redox potential ($K_4[Fe(CN)_6]$), Prussian Blue nanoparticles display the highest selectivity toward H_2O_2 in the presence of dissolved oxygen, while for the other electroactive nanomaterials, peroxidase-like activity is comparable with oxidase-like one or even significantly lower (Figure S11).

So, combining the highest catalytic activity among the electroactive nanomaterials with the absence of oxidase-like activity, Prussian Blue-based nanoparticles seem to be the most promising electroactive material for the design of "artificial peroxidase".

Size-Dependent Constants for the Prussian Blue-Based Nanozymes. As mentioned, the porosity and specific surface area of Prussian Blue based nanozymes are practically independent of their diameter. Besides, Prussian Blue based nanostructures possess sufficient electronic conductivity. So, in contrast to oxide-based catalysts, for which the catalytic reaction occurs only on the surface, the ensembles of Prussian Blue based active sites are expected to facilitate the catalytic process in the bulk of nanoparticles. To check this assumption, we determined apparent catalytic rate constants per colloidal nanoparticles with different sizes (roughly from 30 to 350 nm) using the steady-state kinetic approach.

Figure 4 displays catalytic rate constants for reducing substrates, which are obviously dependent on the rate of

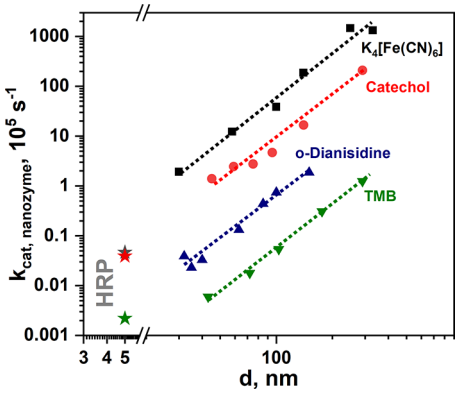

Figure 4. Dependence of k_{cat} for different reducing substrates on the sizes of catalytically synthesized Prussian Blue based nanozymes, 2.0 mM H_2O_2, 0.05 M citrate-phosphate buffer, pH 5.0. The values for enzyme peroxidase under similar conditions are indicated with stars.

H_2O_2 activation. Expectedly, these constants are size-dependent, tending to be proportional to the overall number of electroactive sites constituting the nanoparticle independently of the reducing substrate. The linear regression of the dependencies in double-logarithmic plots returns the slopes varying from 2.6 to 2.8, indicating that hydrogen peroxide penetrates the bulk of the particle. As a result, even the smallest

https://doi.org/10.1021/acsami.5c07510
ACS Appl. Mater. Interfaces 2025, 17, 40964−40973

Prussian Blue-based nanozymes display catalytic rate constants up to 40 times higher than for horseradish peroxidase.

A slight diminishing of catalytic rate constants for the largest particles in the presence of $K_4[Fe(CN)_6]$ can be due to the rate of the intrananozyme electron transfer becoming comparable to the electrocatalyst interaction with the "fastest" substrate.[24] As mentioned above, BET specific surface area even increases slightly for the larger particles; the observed effect, thus, cannot be associated with a nonuniform microstructure throughout the nanoparticle volume. Nevertheless, the observed inclusion of such a great number of active sites even for the largest nanoparticles probably indicates that the process is rather limited by the diffusion of H_2O_2 and its reduction than by electron conductivity and interaction with the reducing substrate. The latter, as we have shown earlier, turns out to be the fastest step of the catalytic cycle in the case of Prussian Blue-based nanozymes.[24] It promises high electrocatalytic activity of immobilized nanoparticles, proportional to their surface concentration.

In addition, we evaluated the oxidase-like activity for Prussian Blue-based nanozymes of different sizes. Similarly to peroxidase-like activity, in the case of substrate oxidation with oxygen, catalytic rate constants for reducing substrate increase with particle size, returning the slope of about 2.7−2.9 in bilogarithmic plots (Figure S12). In other words, oxygen penetrates the electrocatalyst—as a result, oxygen reduction reaction occurs both at the surface and in the bulk of the nanoparticle. Since the slopes of the size dependences for the catalytic rate constants of peroxidase-like and oxidase-like activities practically coincide, the selectivity toward H_2O_2 in the presence of dissolved oxygen turns out to be practically independent of the nanoparticles' diameter.

Size-Dependent Electrochemical Constant. Being immobilized onto the inert electrode surfaces, peroxidases can be involved in direct (mediator-free) bioelectrocatalysis,[18] resulting in H_2O_2 electrochemical sensors. In contrast to enzymes, electroactive nanoparticles represent ensembles of active sites, which can be simultaneously involved in (electro)catalytic reactions. Moreover, due to a uniformly accessible electroactive surface, they do not require special immobilization protocols for the proper orientation or electron transfer facilitation. We expect that superior catalytic constants for catalytically synthesized Prussian Blue-based nanozymes would provide their high electrocatalytic activity.

The electrochemical rate constants (k_{el}) of H_2O_2 reduction were determined for the nanozymes adsorbed on the surface of glassy carbon electrodes. To separate the current terms controlled by diffusion and kinetics, we registered the signal of H_2O_2 reduction with the nanozyme-modified electrodes integrated into the wall-jet cell upon varying the flow rate v (Figure S13). The dependencies of the current density on v registered in the presence of different H_2O_2 concentrations were linearized in Koutecky−Levich type plots valid for the wall-jet cell (j^{-1} vs $v^{-0.75}$).[25] The set of slopes and intercepts of the registered dependencies represents the diffusion and the kinetic components of the reciprocal current, which linearly depend on the H_2O_2 content (Figure 5a). The electrochemical rate constants were calculated using the slope of the kinetic term j_k − H_2O_2 concentration dependency as described in ref 25. We expect that due to the high electroactivity of Prussian Blue, the bulk of the adsorbed nanozymes is involved in electrocatalysis (at least partially). Accordingly, we modified the electrode surfaces with different amounts of nanozymes. As

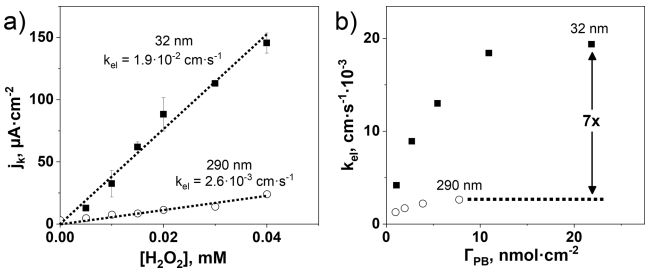

Figure 5. (a) Dependence of the kinetic component of the current density on the concentration of H_2O_2 for the Prussian Blue based nanozymes with the size of 32 nm (box solid) and 290 nm (circle open) adsorbed at the glassy carbon electrodes. (b) Dependence of electrochemical constants on the surface concentration of electroactive Prussian Blue, consisting of nanozymes with different sizes.

shown, k_{el} is indeed proportional to the amount of immobilized Prussian Blue, reaching the saturation at high values (probably due to limited electron transport at the electrodelelectrocatalyst interface) (Figure 5b).

For the coatings based on 32 nm nanozymes, the limiting constant values appeared to be ∼7 times higher than those for the layers based on nanoparticles with a diameter of 290 nm. Such a phenomenon can hardly be attributed to crystal plane orientation in the Prussian Blue nanoparticles due to rather poor crystallinity of the samples, resulting in their isotropic characteristics (Figure 1d−f). It probably can be explained by a larger contact area of smaller nanozymes with each other and the electrode surface. The achieved ultimate values of the electrochemical constants (∼1.9 × 10^{-2} cm·s^{-1}) are two times higher than those for the electrodes modified with continuous Prussian Blue films[25] and 2 orders of magnitude higher than for the magnetite-modified electrodes.[26] Such excellent electrocatalytic properties of the interfaces modified with the catalytically synthesized Prussian Blue-based nanozymes would allow them to be applied for the construction of highly sensitive H_2O_2 sensors.

Cytotoxicity and ROS Scavenging Activity of Prussian Blue-Based "Artificial Peroxidase". Inflammation plays a significant role in a number of life-threatening acute and chronic conditions, including cardiovascular, respiratory, neurodegenerative, and autoimmune diseases.[27] An increase in inflammatory cell-derived ROS, leading to redox imbalance, escalates oxidative stress and triggers secondary inflammation.[28] Thus, maintaining redox homeostasis is an important method to relieve the inflammatory reaction. Nanozymes with peroxidase-like activity, continuously decomposing excessive ROS through catalytic reactions and modulating inflammatory responses, have demonstrated significant potential in treating ROS-related disorders.[29] In contrast to natural peroxidases, which tend to be rapidly hydrolyzed by proteases and thus inapplicable for anti-inflammatory treatment, nanozymes are expected to be more stable in living organisms. From this point of view, catalytically synthesized Prussian Blue-based nanozymes, demonstrating the highest catalytic activity among the electroactive peroxidase mimetics, appear to be a promising nanomedication for inflammation-related disease therapy.

Despite Prussian Blue being recognized as a safe antidote for radioactive thallium and cesium-137 poisoning, we first investigated the biocompatibility of its catalytically synthesized nanoparticles. Cytotoxicity of the Prussian Blue-based nanozymes with sizes of 32 and 290 nm toward murine macrophage

https://doi.org/10.1021/acsami.5c07510
ACS Appl. Mater. Interfaces 2025, 17, 40964−40973

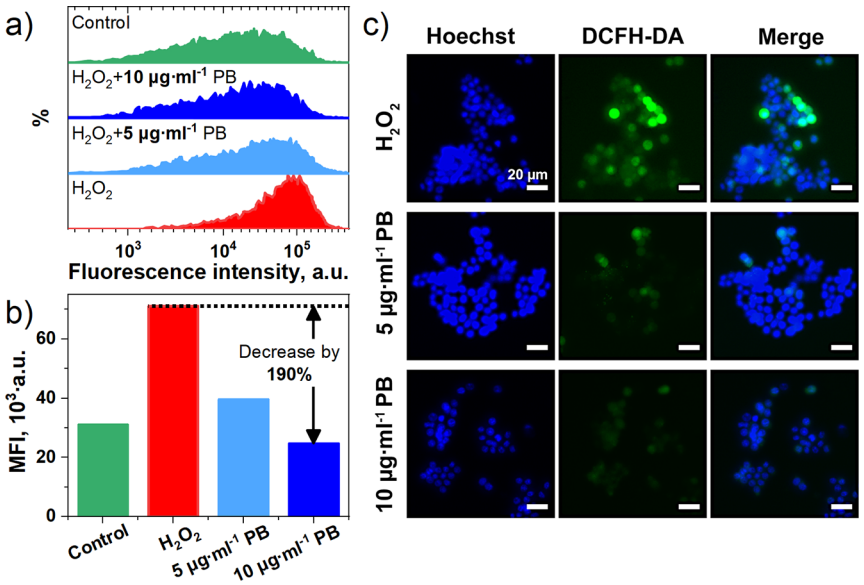

Figure 6. (a) ROS scavenging activities of Prussian Blue NPs in 100 μm H_2O_2 stimulated RAW 264.7 cells investigated by determined with flow cytometry. (b) Mean fluorescence of the DCFH-DA in RAW 264.7 cells after incubation in the presence of Prussian Blue NPs determined using flow cytometry; ROS-excess was stimulated by 100 μm H_2O_2. (c) Visualization of intracellular ROS scavenging in RAW 264.7 cells treated with different concentrations of Prussian Blue NPs: micrographs with fluorescence detection of the cells stained with Hoechst and ROS stained with DCFH-DA dyes obtained using a confocal microscope.

RAW 264.7 was tested using the cell counting kit assay. Within the error tolerances, the cell viability in the course of 24 h incubation slightly depends on the Prussian Blue nanoparticle's size and its concentration up to 43 $\mu g \cdot mL^{-1}$, while a significant change in cytotoxicity is observed only at concentrations of 86 $\mu g \cdot mL^{-1}$ (Figure S14). A similar trend in cytotoxicity is observed upon a long-term (>48 h) incubation of cells with the nanozymes, while the cell viability is slightly (within 5%) lower (Figure S15). Probably, the observed decrease in cell viability is mainly associated with the concentration of nanozymes, rather than their decomposition in the cell medium with time.

The RAW 264.7 cells incubated with Prussian Blue-based nanozymes for 3 h were then treated with 100 μM H_2O_2 for 30 min. Presumably, the presence of proteins in cell culture media would stabilize the smaller size of nanoparticles. As we have shown earlier, the apparent catalytic constant per a single redox-active site is practically independent of the nanozyme size in the case of small particles (below 100 nm).[24] Accordingly, the total activity (per mass of medication) is expected to remain unchanged. The intracellular ROS was further quantitatively analyzed by flow cytometry. DCFH-DA diffusing through the cell membrane into the cytosol is hydrolyzed by intracellular esterases to DCFH trapped inside the cells. Nonfluorescent DCFH reacting with free radical compounds proportionally generates the fluorescent 2′,7′-dichlorofluorescein (DCF). Accordingly, flow cytometric detection of DCF fluorescence provides information on reactive oxygen species amounts in single cells. The distributions of the cell number by their fluorescence intensity, normalized to their total count for different conditions, are given in Figure 6a.

The integral values of mean fluorescence intensity (MFI) calculated considering the fraction of cells with the given intensity ($MFI = \sum(\text{intensity})_i \times N_i/N$, where N is the total count of cells) are represented in Figure 6b. The calculated MFI values indicate that catalytically synthesized Prussian Blue-based nanozymes exhibit a dose-dependent H_2O_2 scavenging capacity (Figure 6a). The latter reaches its saturation using nanozyme concentrations above 10 μg mL^{-1}, which is 4−5 times lower than the cytotoxicity threshold (Figures S14 and S15). The efficacy of ROS scavenging with Prussian Blue-based nanozymes was confirmed with fluorescence imaging by a confocal microscope (Figure 6c). MFI for the peroxide-treated cells incubated with nanozymes appears to be even slightly lower than that for the nontreated cells, modeling the healthy ones (control group). It probably points to a nonzero level of reactive oxygen species in the nontreated RAW 264.7 cells. Accordingly, the lowest MFI value achieved for the cells incubated with Prussian Blue-based nanozymes can be considered as zero. As shown, the ultimate ROS scavenging activity results in up to 190% decrease of H_2O_2 level compared to peroxide-treated cells incubated without nanozymes (Figure 6b). It indicated high ROS scavenging activity of the catalytically synthesized Prussian Blue-based nanozymes.

4. CONCLUSIONS

With the current research, we clearly show that peroxidase-like activity of transition metal-based nanomaterials is associated with their redox reactions. Such nanomaterials act as redox catalysts: while their initial form is silent in catalysis, transition metal ion reduction converts them to a catalytically active state. Catalytic constants are thus determined by the difference in the formal redox potentials of the nanozyme material and the reducing substrate. At the same time, high electroactivity allows the inclusion of a large number of active sites in both catalytic and electrocatalytic reactions.

A unified investigation of a set of electroactive nanomaterials clearly shows the advantages of catalytically synthesized Prussian Blue based nanozymes: (1) ultrahigh catalytic activity belonging to a single trend with natural HRP depending on the difference between the catalyst and the substrate redox potentials; (2) the lowest oxidase activity among the considered nanozymes even in the presence of the substrates

https://doi.org/10.1021/acsami.5c07510
ACS Appl. Mater. Interfaces 2025, 17, 40964−40973

with high electron-donor ability; (3) involvement into catalysis of a great number of assembled active sites even in the bulk of nanozymes, resulting in their high activity; (4) record size-dependent electrochemical constants for H_2O_2 reduction reaction, exceeding those for HRP involved in direct electrocatalysis; (5) absence of cytotoxicity and high ROS scavenging activity. In addition to H_2O_2 sensing and anti-inflammatory therapy, discussed in the article, such nanozymes can, in prospect, substitute peroxidase as labels for various analytical platforms with optical or electrochemical readout.

We believe that unraveled peculiarities in redox catalysis with inorganic nanomaterials give insight into the limits of catalysis with different nanozymes. The established principles are universal and can guide further development and application of various nanozymes, not limited to peroxidases.

■ ASSOCIATED CONTENT

Supporting Information

The Supporting Information is available free of charge at https://pubs.acs.org/doi/10.1021/acsami.5c07510.

Image of reaction mixture upon Prussian Blue nanoparticles formation in course of catalytic synthesis; X-ray powder diffraction patterns of nanozymes; nanozymes' hydrodynamic size distributions; BET adsorption results; half-wave potentials of H_2O_2 reduction as a function of nanozyme redox potentials; electroactivity of Fe_3O_4; XPS data for nanozymes; examples of initial reaction rate dependence on the substrate, nanozymes or H_2O_2 concentrations; extended dependence of k_{cat} on the difference between the redox potentials of o-phenylenediamine and nanozymes; selectivity of nanozymes; oxidase-like activity of Prussian Blue based nanozymes as a function of their size; kinetic studies of H_2O_2 electrocatalytic reduction onto the Prussian Blue-based nanozymes; cytotoxicity of Prussian Blue based depending on their size; concentration and time of incubation (PDF)

■ AUTHOR INFORMATION

Corresponding Author

Maria A. Komkova − *Chemistry faculty of M.V. Lomonosov Moscow State University, Moscow 119991, Russia;* orcid.org/0000-0002-9103-9984; Email: komkovama@my.msu.ru

Authors

Aleksandra A. Shneiderman − *Materials Science faculty of M.V. Lomonosov Moscow State University, Moscow 119991, Russia*

Elena S. Povaga − *Materials Science faculty of M.V. Lomonosov Moscow State University, Moscow 119991, Russia*

Yuting Wang − *Department of Biomedical Engineering, College of Engineering and Applied Sciences, Nanjing National Laboratory of Microstructures, Jiangsu Key Laboratory of Artificial Functional Materials, Nanjing University, Nanjing 210023 Jiangsu, China*

Xiwen Chen − *Department of Biomedical Engineering, College of Engineering and Applied Sciences, Nanjing National Laboratory of Microstructures, Jiangsu Key Laboratory of Artificial Functional Materials, Nanjing University, Nanjing 210023 Jiangsu, China*

Alexander L. Kustov − *Chemistry faculty of M.V. Lomonosov Moscow State University, Moscow 119991, Russia;* orcid.org/0000-0003-0869-8784

Congzhong Yang − *Department of Biomedical Engineering, College of Engineering and Applied Sciences, Nanjing National Laboratory of Microstructures, Jiangsu Key Laboratory of Artificial Functional Materials, Nanjing University, Nanjing 210023 Jiangsu, China*

Hui Wei − *Department of Biomedical Engineering, College of Engineering and Applied Sciences, Nanjing National Laboratory of Microstructures, Jiangsu Key Laboratory of Artificial Functional Materials, Nanjing University, Nanjing 210023 Jiangsu, China;* orcid.org/0000-0003-0870-7142

Arkady A. Karyakin − *Chemistry faculty of M.V. Lomonosov Moscow State University, Moscow 119991, Russia*

Complete contact information is available at: https://pubs.acs.org/10.1021/acsami.5c07510

Notes

The authors declare no competing financial interest.

■ ACKNOWLEDGMENTS

Financial support through Russian Science Foundation Grant 24-13-00049, https://rscf.ru/project/24-13-00049/, is acknowledged. The research was carried out using the equipment of MSU Shared Research Equipment Center "Technologies for obtaining new nanostructured materials and their complex study" and purchased by MSU in the frame of the MSU Program of Development.

■ ABBREVIATIONS

BET,Brunauer−Emmett−Teller; DCF,2′,7′-dichlorofluorescein; DCFH,2′,7′-dichlorodihydrofluorescein; DCFH-DA,2′-7′-dichlorodihydrofluorescein diacetate; HRP,horseradish peroxidase; PDI,polydispersity index; TMB,3,3′,5,5′-tetramethylbenzidine; XPS,X-ray photoelectron spectroscopy

■ REFERENCES

(1) Manea, F.; Houillon, F. B.; Pasquato, L.; Scrimin, P. Nanozymes: Gold-Nanoparticle-Based Transphosphorylation Catalysts. *Angew. Chemie Int. Ed.* **2004**, *43* (45), 6165−6169.

(2) Yan, X.*Nanozymology*; Nanostructure Science and Technology; Springer Singapore: Singapore, 2020. .

(3) Gao, L.; Zhuang, J.; Nie, L.; Zhang, J.; Zhang, Y.; Gu, N.; Wang, T.; Feng, J.; Yang, D.; Perrett, S.; Yan, X. Intrinsic Peroxidase-like Activity of Ferromagnetic Nanoparticles. *Nat. Nanotechnol.* **2007**, *2* (9), 577−583.

(4) Wu, J.; Wang, X.; Wang, Q.; Lou, Z.; Li, S.; Zhu, Y.; Qin, L.; Wei, H. Nanomaterials with Enzyme-like Characteristics (Nanozymes): Next-Generation Artificial Enzymes (II). *Chem. Soc. Rev.* **2019**, *48* (4), 1004−1076.

(5) Karyakin, A. A. Catalytic Properties of Peroxidase Mimicking Nanozymes. *Russ. Chem. Rev.* **2023**, *92* (8), No. RCR5088.

(6) Scott, S.; Zhao, H.; Dey, A.; Gunnoe, T. B. Nano-Apples and Orange-Zymes. *ACS Catal.* **2020**, *10* (23), 14315−14317.

(7) Lyu, Y.; Scrimin, P. Mimicking Enzymes: The Quest for Powerful Catalysts from Simple Molecules to Nanozymes. *ACS Catal.* **2021**, *11* (18), 11501−11509.

(8) Weiss, J. The Catalytic Decomposition of Hydrogen Peroxide on Different Metals. *Trans. Faraday Soc.* **1935**, *31* (0), 1547−1557.

(9) Zheng, J.-J.; Zhu, F.; Song, N.; Deng, F.; Chen, Q.; Chen, C.; He, J.; Gao, X.; Liang, M. Optimizing the Standardized Assays for

Determining the Catalytic Activity and Kinetics of Peroxidase-like Nanozymes. *Nat. Protoc.* **2024**, *19* (12), 3470−3488.
(10) Jiang, B.; Duan, D.; Gao, L.; Zhou, M.; Fan, K.; Tang, Y.; Xi, J.; Bi, Y.; Tong, Z.; Gao, G. F.; Xie, N.; Tang, A.; Nie, G.; Liang, M.; Yan, X. Standardized Assays for Determining the Catalytic Activity and Kinetics of Peroxidase-like Nanozymes. *Nat. Protoc.* **2018**, *13* (7), 1506−1520.
(11) Komkova, M. A.; Karyakina, E. E.; Karyakin, A. A. Catalytically Synthesized Prussian Blue Nanoparticles Defeating Natural Enzyme Peroxidase. *J. Am. Chem. Soc.* **2018**, *140* (36), 11302−11307.
(12) Pourbaix, M.*Atlas of Electrochemical Equilibria in Aqueous Solutions*; National Association of Corrosion 1966, .
(13) Gumpelmayer, M.; Nguyen, M.; Molnár, G.; Bousseksou, A.; Meunier, B.; Robert, A. Magnetite Fe 3 O 4 Has No Intrinsic Peroxidase Activity, and Is Probably Not Involved in Alzheimer's Oxidative Stress. *Angew. Chemie Int. Ed.* **2018**, *57* (45), 14758−14763.
(14) Shcherbakov, A. B. CeO2 Nanoparticles and Cerium Species as Antiviral Agents: Critical Review. *Eur. J. Med. Chem. Reports* **2024**, *10*, No. 100141.
(15) Liu, Y.; Yan, X.; Wei, H.; Gu, N. Medical Nanozymes for Therapeutics. *Nanomedicine* **2023**, 285−329.
(16) Ma, Y.; Tian, Z.; Zhai, W.; Qu, Y. Insights on Catalytic Mechanism of CeO2 as Multiple Nanozymes. *Nano Res.* **2022**, *15* (12), 10328−10342.
(17) Yu, Y.; Zhao, S.; Gu, D.; Zhu, B.; Liu, H.; Wu, W.; Wu, J.; Wei, H.; Miao, L. Cerium Oxide Nanozyme Attenuates Periodontal Bone Destruction by Inhibiting the ROS−NFκB Pathway. *Nanoscale* **2022**, *14* (7), 2628−2637.
(18) Yaropolov, A. I.; Malovik, V. M.; Varfolomeev, S. D.; Berezin, I. V. Electroreduction of Hydrogen Peroxide on an Electrode with Immobilized Peroxidase. *Dokl. Akad. Nauk SSSR* **1979**, *249* (6), 1399−1401.
(19) Komkova, M. A.; Zarochintsev, A. A.; Karyakina, E. E.; Karyakin, A. A. Electrochemical and Sensing Properties of Prussian Blue Based Nanozymes "Artificial Peroxidase". *J. Electroanal. Chem.* **2020**, *872*, No. 114048.
(20) Sitnikova, N. A.; Komkova, M. A.; Khomyakova, I. V.; Karyakina, E. E.; Karyakin, A. A. Transition Metal Hexacyanoferrates in Electrocatalysis of H2O2 Reduction: An Exclusive Property of Prussian Blue. *Anal. Chem.* **2014**, *86* (9), 4131−4134.
(21) Bard, A. J.; Faulkner, L. R.; White, H. S.*Electrochemical Methods: Fundamentals and Applications*; John Wiley & Sons 2022
(22) Andreu, R.; Ferapontova, E. E.; Gorton, L.; Calvente, J. J. Direct Electron Transfer Kinetics in Horseradish Peroxidase Electrocatalysis. *J. Phys. Chem. B* **2007**, *111* (2), 469−477.
(23) Zhao, Y.; Chu, X.; Yang, B. Electrochemical Behavior of Hemin Binding with Human Centrin 3. *Bioelectrochemistry* **2017**, *117*, 15−22.
(24) Komkova, M. A.; Kostyukov, A. A.; Shneiderman, A. A.; Kuzmin, V. A.; Karyakin, A. A. Fast Reaction of the Prussian Blue Based Nanozyme "Artificial Peroxidase" with the Substrates: Pre-Steady-State Kinetic Approach. *J. Phys. Chem. Lett.* **2024**, *15* (34), 8642−8649.
(25) Karyakin, A. A.; Karyakina, E. E.; Gorton, L. The Electrocatalytic Activity of Prussian Blue in Hydrogen Peroxide Reduction Studied Using a Wall-Jet Electrode with Continuous Flow. *J. Electroanal. Chem.* **1998**, *456* (1−2), 97−104.
(26) Lin, M. S.; Leu, H. J. A Fe3O4-Based Chemical Sensor for Cathodic Determination of Hydrogen Peroxide. *Electroanalysis* **2005**, *17* (22), 2068−2073.
(27) Forrester, S. J.; Kikuchi, D. S.; Hernandes, M. S.; Xu, Q.; Griendling, K. K. Reactive Oxygen Species in Metabolic and Inflammatory Signaling. *Circ. Res.* **2018**, *122* (6), 877−902.
(28) Yu, W.; Tu, Y.; Long, Z.; Liu, J.; Kong, D.; Peng, J.; Wu, H.; Zheng, G.; Zhao, J.; Chen, Y.; Liu, R.; Li, W.; Hai, C. Reactive Oxygen Species Bridge the Gap between Chronic Inflammation and Tumor Development. *Oxid. Med. Cell. Longev.* **2022**, *2022*, No. 2606928.
(29) Wang, X.; Wang, Z.-D.; Hu, S.-Y.; Ding, X.; Hu, Y.-J. Regulator of Oxidative Balance: Research Progress of Nanozymes in ROS-Related Diseases. *Mater. Today Chem.* **2025**, *44*, No. 102540.

https://doi.org/10.1021/acsami.5c07510
ACS Appl. Mater. Interfaces 2025, 17, 40964−40973